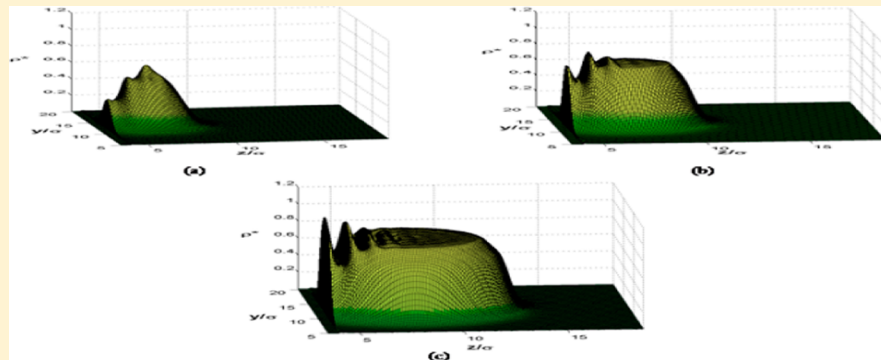


Three-Dimensional Density Functional Study of Heterogeneous Nucleation of Droplets on Solid Surfaces

Di Zhou, Jianguo Mi,* and Chongli Zhong

State Key Laboratory of Organic–Inorganic Composites, Beijing University of Chemical Technology, Beijing 100029, China



ABSTRACT: We present a three-dimensional density functional approach to investigate heterogeneous nucleation behaviors of Lennard-Jones fluid on solid walls. In the theoretical calculation, fast Fourier transforms to compute the convolutions of Euler–Lagrange equation enables a high-efficient algorithm in three-dimensional space. The density distributions of a growing nucleus are presented to account for the nucleation process. Accordingly, the structures of nucleated droplet and surrounding supersaturated vapor on different walls are analyzed, and the corresponding free energy barriers and the critical radii are obtained to evaluate the difficulty of droplet formation. Since the theoretical approach is strictly constructed in three-dimensional space, and the liquid–solid, vapor–solid, and vapor–liquid interfacial tensions as well as the vapor–liquid–solid line tension are entirely integrated into the excess free energy expression, the present approach provides a flexible and efficient tool for studying heterogeneous nucleation.

1. INTRODUCTION

Heterogeneous nucleation normally occurs on the surfaces of solid substrates or foreign particles. It occurs much more often than homogeneous nucleation in nature since the presence of a wall/particle facilitates nucleation and reduces the energy barrier. The droplet nucleation on solid surfaces plays a significant role in heat transfer¹ and vapor deposition.^{2,3} Although considerable empirical knowledge has been accumulated, many questions remain. Since nucleation droplet merely consists of a few hundred or thousand molecules, experiments are hard to control and the nucleation sites can only be observed indirectly.⁴ The process and mechanism of heterogeneous nucleation need to be further clarified. In this regard, understanding the fundamentals of heterogeneous nucleation through theoretical routes is crucial to achieve control over these properties.

The most widespread approach is the classical heterogeneous nucleation theory, which was originally developed by Volmer⁵ and revised by Gortz.⁶ As a macroscopic thermodynamic theory, it depends on the density and the surface tension of bulk liquid. It has shown that the theory cannot correctly describe the properties of heterogeneous nucleation in some cases,^{7,8} where the surface tension is ill-defined since the surface enrichment or depletion effect induced by the solid surface is not taken into account. Meanwhile, the mechanical and thermodynamic treatments of the traditional macroscopic theory have difficulties

in consideration of the three-phase contact line tension. On the other hand, a number of differences between theoretical predictions and experimental results suggest that nucleation does not proceed via the classical pathway but follows more complex routes.⁹

In recent years, molecular simulation has been a powerful tool to study the physical behavior of droplet nucleation and growth at the microscopic level. Although heterogeneous nucleation has not been researched as widely as homogeneous nucleation by simulation techniques, there exist some reports on molecular simulations of heterogeneous nucleation. For examples, Kimura and co-workers^{10,11} performed the molecular dynamics simulations to access the equilibrium liquid droplet on the solid surface, and obtained the relationship between the potential parameter of molecules and the contact angle. Rozas and Kraska¹² reported the heterogeneous nucleation and growth of supersaturated argon vapor at polyethylene surfaces from molecular dynamics simulations. Winter et al.^{4,13} computed the heterogeneous nucleation barriers to test the classical theory for the lattice gas model using Monte Carlo simulations and found that the classical theory is relatively accurate if the line tension correction

Received: August 7, 2012

Revised: October 10, 2012

Published: November 8, 2012

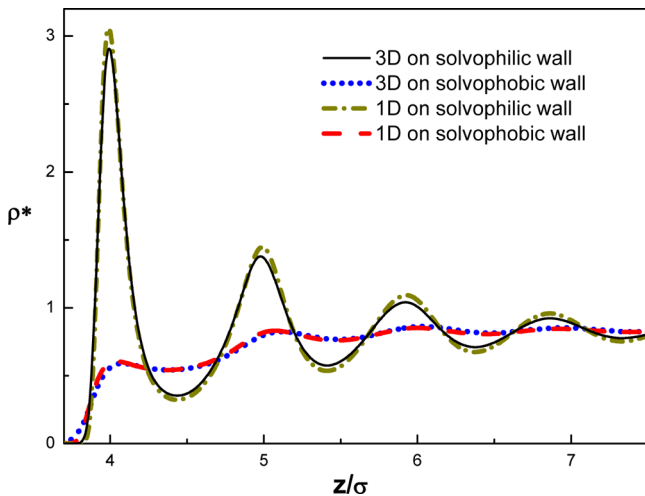


Figure 1. Density profiles of LJ fluid on solvophilic ($\epsilon_{fw} = 0.80\epsilon$) and supersolvophobic ($\epsilon_{fw} = 0.14\epsilon$) walls given by 3D-DFT and 1D-DFT, respectively. The bulk density is $\rho_b^* = 0.833$.

is considered. The simulation method yields reliable results for heterogeneous nucleation. However, it is usually quite time-consuming because the trajectories of many particles are followed over long time periods to calculate averaged quantities of the system.

Statistical mechanical theories provide a potential way to describe heterogeneous nucleation from the microscopic point of view. Of various theoretical approaches, classical density functional theory (DFT) has been successfully applied to adsorption, wetting, layering transition, and capillary condensation at planar and nonplanar substrates.^{14,15} The key issue of DFT is to derive an expression for the grand potential. By minimizing the grand potential, the structure of the nucleated droplet and the surrounding supersaturated vapor can be determined, and the excess free energy of the system can be easily obtained. The priority of DFT over other mean field theories is attributed to its accurate density and energy distributions for heterogeneous system. Talanquer and Oxtoby⁷ first studied a cylindrical symmetrical droplet of van der Waals fluid on a solid surface by a density functional approach. They concluded that classical nucleation theory was inadequate as the spinodal is approached. Bykov and Zeng^{16,17} developed a hybrid thermodynamic/density functional model to treat the heterogeneous nucleation of Lennard-Jones (LJ) fluid on mesoscopic wettable particles and obtained the important characteristics of heterogeneous nucleation, including the formation free energy of the droplet and nucleation barrier height. DFT emerges as an auspicious perspective for heterogeneous nucleation.

For the other microscopic description, Ruckenstein and co-workers extended the kinetic theory of nucleation from homogeneous nucleation^{18,19} to heterogeneous nucleation.²⁰ Very recently, they studied the effect of the nonuniform fluid density distribution in the nucleus on the heterogeneous nucleation of liquid at different solid surfaces and concluded that the nonuniformity decreases the nucleation rate when compared to the uniform density distribution. Nevertheless, the density distribution is determined on the basis of the DFT approach.²¹

In our previous investigations, a nonlocal DFT approach²² has been well developed by integration of the modified fundamental measure theory²³ for short-range repulsion and the weighted density approximation²⁴ for long-range attraction. The ability of the improved DFT for predicting homogeneous nucleation has

also been validated.²⁵ In this paper, we extend it to the three-dimensional (3D) space to present an all-around analysis of droplet formation on solid walls. Unlike the classical nucleation theory, in which the planar liquid–vapor interfacial tension is the crucial input, the contributions from the surface force²⁶ arising from the fluid–solid interactions and from the curvature of the droplet to the excess free energy of nucleation have been taken fully into account. Following Knepley et al.,²⁷ we provide a full numerical strategy for studying the heterogeneous behaviors. In 3D-DFT, the algorithm employs fast Fourier transforms to compute the convolutions of the Euler–Lagrange equation and Picard iteration with line search to solve the equation. This algorithm can extensively save computational time and memory usage. The density distributions at liquid–solid, vapor–solid, and vapor–liquid interfaces during the process of nucleation are quantitatively calculated. Accordingly, the critical radii and the free energy barriers of droplet condensed from supersaturated vapor are evaluated on different walls.

2. THEORY

For simplicity, the vapor, liquid and solid wall particles are characterized by the LJ interaction potential

$$u(r) = 4\epsilon \left[\left(\frac{\sigma}{r} \right)^{12} - \left(\frac{\sigma}{r} \right)^6 \right] \quad (1)$$

where ϵ and σ are the LJ energy and length parameters. In this work, the wall is invariant in the x and y directions, the fluid–solid interactions only depend on z . The overall potential exerted by the wall can be described by the Steele-type 10-4 potential²⁸

$$V_{ext}(z) = 2\pi\epsilon_{fw}\sigma_{fw}^2 \left[\frac{2}{5} \left(\frac{\sigma_{fw}}{z} \right)^{10} - \left(\frac{\sigma_{fw}}{z} \right)^4 \right] \quad (2)$$

in which ϵ_{fw} and σ_{fw} are the fluid–wall potential parameters and σ_{fw} is set to be σ . In this work, σ and ϵ are the diameter and energy scale of a fluid particle and are taken as length and energy units.

In general, the grand potential $\Omega[\rho(\mathbf{r})]$ of a three-phase system can be expressed as the following form:

$$\begin{aligned} \Omega[\rho(\mathbf{r})] = & k_B T \int d\mathbf{r} \rho(\mathbf{r}) [\ln(\rho(\mathbf{r})\Lambda^3) - 1] + F_{hs}[\rho(\mathbf{r})] \\ & + F_{att}[\rho(\mathbf{r})] + \int d\mathbf{r} [\rho(\mathbf{r})(V_{ext}(\mathbf{r}) - \mu)] \end{aligned} \quad (3)$$

where $\rho(\mathbf{r})$ presents the density distribution with configuration \mathbf{r} , $F_{hs}[\rho(\mathbf{r})]$ stands for the local Helmholtz free energy of hard-sphere reference system, $F_{att}[\rho(\mathbf{r})]$ accounts for the local Helmholtz free energy of the attractive contribution, $V_{ext}(\mathbf{r})$ denotes the fluid–wall potential, and μ indicates the chemical potential of the bulk fluid, which can be derived as $\rho(\mathbf{r}) = \rho_b$. In addition, k_B is the Boltzmann constant, T is the absolute temperature, and $\Lambda = (2\pi mk_B T/h^2)^{1/2}$ is the thermal de Broglie wavelength. For the homogeneous system, $V_{ext}(\mathbf{r}) = 0$.

For a system with a fixed number of molecules, the equilibrium 3D density profile of the system can be obtained by minimizing the grand potential and solving the Euler–Lagrange equation

$$\rho(\mathbf{r}) = \Lambda^{-3} \exp \left(\beta\mu - \beta \frac{\delta(F_{hs}[\rho(\mathbf{r})] + F_{att}[\rho(\mathbf{r})])}{\delta\rho(\mathbf{r})} - \beta V_{ext}(\mathbf{r}) \right) \quad (4)$$

with $\beta = 1/k_B T$.

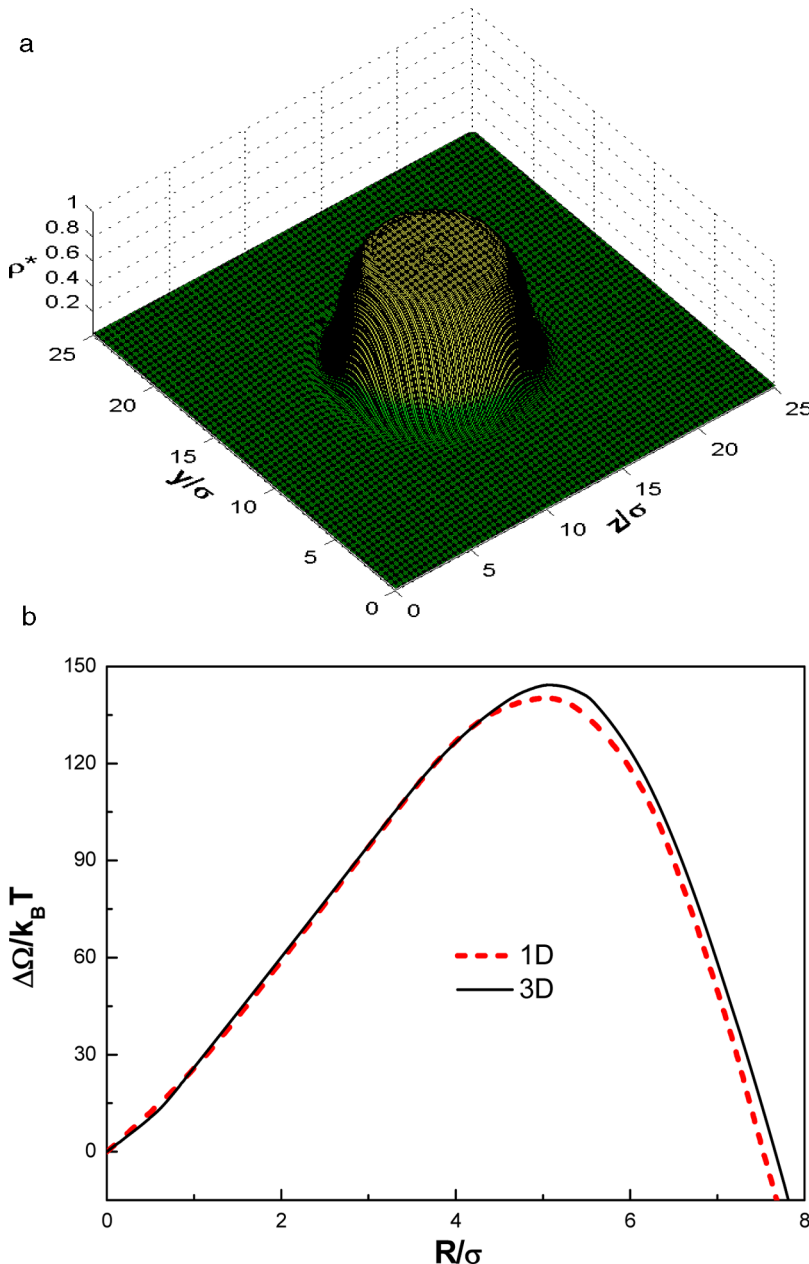


Figure 2. (a) Two-dimensional cut of density profiles of LJ fluid under the condition of the critical nucleation. (b) Comparison of free energy and critical radius of homogeneous nucleation given by 3D-DFT and 1D-DFT, respectively. The profiles are cut at $x = 12.8\sigma$.

According to the modified fundamental measure theory,²³ the hard sphere contribution can be represented by

$$\beta F_{hs}[\rho(\mathbf{r})] = \int \Phi_{hs}[n_\alpha(\mathbf{r})] d\mathbf{r} \quad (5)$$

in which $\Phi_{hs}[n_\alpha(\mathbf{r})]$ is the Helmholtz free energy density of the hard sphere fluid and can be written as

$$\begin{aligned} \Phi_{hs}[n_\alpha(\mathbf{r})] = & -n_0 \ln(1 - n_3) + \frac{n_1 n_2 - \mathbf{n}_{V1} \cdot \mathbf{n}_{V2}}{1 - n_3} \\ & + \frac{1}{36\pi} \left(n_3 \ln(1 - n_3) + \frac{n_3^2}{(1 - n_3)^2} \right) \\ & \times \frac{n_2^3 - 3n_2 \mathbf{n}_{V2} \cdot \mathbf{n}_{V2}}{n_3^3} \end{aligned} \quad (6)$$

In 3D space, n_α integrals can be calculated using the fast Fourier transform and the convolution theorem

$$n_\alpha(\mathbf{r}) = \int \rho(\mathbf{r}') w^{(\alpha)}(\mathbf{r}' - \mathbf{r}') d\mathbf{r}' = \mathcal{F}^{-1}(\tilde{\rho}(\mathbf{k}) \cdot \tilde{w}^{(\alpha)}(\mathbf{k})) \quad (7)$$

where \mathcal{F} denotes the Fourier transform operator and the tilde notation means the Fourier image of the function. The weight functions $\tilde{w}^{(\alpha)}(\mathbf{k})$, $\alpha = 0, 1, 2, 3, V1$, and $V2$ are given by²⁷

$$\tilde{w}^{(2)}(\mathbf{k}) = \pi d^2 \tilde{w}^{(0)}(\mathbf{k}) = 2\pi d \tilde{w}^{(1)}(\mathbf{k}) = 2\pi d \sin(kd/2)/k \quad (8)$$

$$\tilde{w}^{(3)}(\mathbf{k}) = \frac{4\pi}{k^3} (\sin(kd/2) - (kd/2) \cos(kd/2)) \quad (9)$$

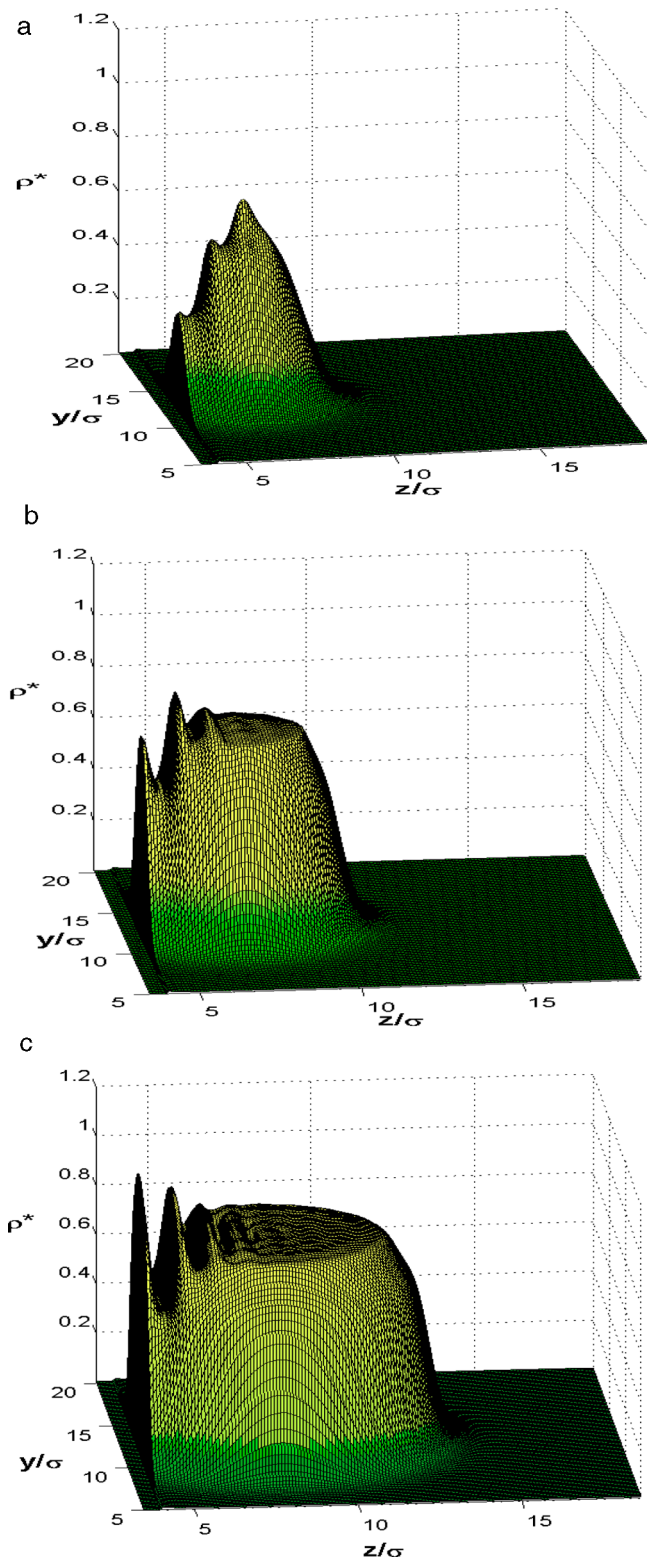


Figure 3. Evaluation of density profile and nucleus radius during the nucleation process of droplet on the supersolvophobic wall with $\theta = 170^\circ$. (a) $R = 2.57\sigma$, (b) $R = 3.56\sigma$, and (c) $R = 4.94\sigma$. The profiles are cut at $x = 12.8\sigma$.

$$\begin{aligned} \tilde{w}^{(V2)}(\mathbf{k}) &= 2\pi d\tilde{w}^{(V1)}(\mathbf{k}) \\ &= \frac{-4\pi i}{k^3} (\sin(kd/2) - (kd/2) \cos(kd/2)) \mathbf{k} \end{aligned} \quad (10)$$

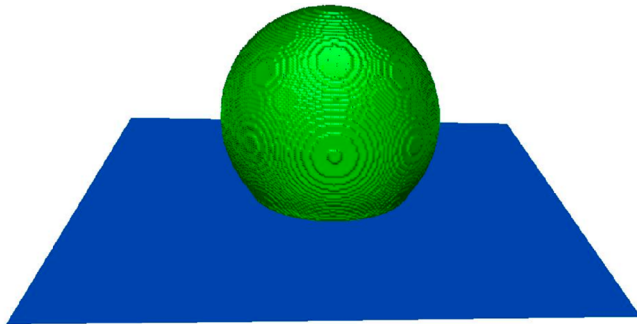


Figure 4. Morphology of critical droplet formed on the supersolvophobic wall with $\theta = 170^\circ$. Only those sites in the droplet ($\rho^* \geq 0.42$) are presented.

where d is the Barker–Henderson diameter.^{29,30} Correspondingly, the hard sphere chemical potential is calculated by

$$\frac{\partial \beta F_{hs}[\rho(\mathbf{r})]}{\partial \rho(\mathbf{r})} = \sum_{\alpha} \int \frac{\partial \Phi_{hs}}{\partial n_{\alpha}} w^{(\alpha)}(\mathbf{r} - \mathbf{r}') d\mathbf{r}' \quad (11)$$

In the same way, $\partial \beta F_{hs}[\rho(\mathbf{r})]/\partial \rho(\mathbf{r})$ in 3D space can be calculated as eq 7, in which ρ is substituted with $\partial \Phi_{hs}/\partial n_{\alpha}$.

The free energy for the attractive contribution, $F_{att}[\rho(\mathbf{r})]$, can be expressed with the weighted density approximation method²⁴

$$F_{att}[\rho(\mathbf{r})] = \int \rho(\mathbf{r}) a_{att}[\bar{\rho}(\mathbf{r})] d\mathbf{r} \quad (12)$$

in which $\bar{\rho}(\mathbf{r})$ is defined via a weight function $\omega_{att}(\mathbf{r})$

$$\bar{\rho}(\mathbf{r}) = \int \rho(\mathbf{r}') \omega_{att}(\mathbf{r} - \mathbf{r}') d\mathbf{r}' \quad (13)$$

$$\omega_{att}(r) = \frac{c_{att}(\mathbf{r})}{\int c_{att}(\mathbf{r}) d\mathbf{r}} \quad (14)$$

where $c_{att}(r)$ is the attractive part of the direct correlation function with the interfacial average density of nucleation.³¹ In 3D space, eq 13 can be written by

$$\bar{\rho}(\mathbf{r}) = \int \rho(\mathbf{r}') \omega_{att}(\mathbf{r} - \mathbf{r}') d\mathbf{r}' = \mathcal{F}^{-1}(\tilde{\rho}(\mathbf{k}) \cdot \tilde{\omega}_{att}(\mathbf{k})) \quad (15)$$

The chemical potential for the attractive interaction is then expressed as

$$\begin{aligned} \frac{\partial \beta F_{att}[\rho(\mathbf{r})]}{\partial \rho(\mathbf{r})} &= \beta a_{att}[\bar{\rho}(\mathbf{r})] + \beta \int \rho(\mathbf{r}') \frac{\delta a_{att}[\bar{\rho}(\mathbf{r}')]}{\delta \bar{\rho}(\mathbf{r}')} \omega_{att} \\ &\quad \times (\mathbf{r} - \mathbf{r}') d\mathbf{r}' \end{aligned} \quad (16)$$

where $a_{att}[\bar{\rho}(\mathbf{r})]$ is the Helmholtz free energy per particle, which can be seen in ref 32. For the second part in the right side of eq 16, it can be evaluated using the Fourier transform in the same way as eq 15 by replacing $\rho(\mathbf{r}')$ with $\rho(\mathbf{r}') \delta a_{att}[\bar{\rho}(\mathbf{r}')]/\delta \bar{\rho}(\mathbf{r}')$.

Under the condition of vapor supersaturation, the heterogeneous nucleation of the droplet is formed on the solid wall. The supersaturation ratio is defined as $S = p/p^0$, where p is the pressure of the supersaturated vapor and p^0 represents the saturation vapor pressure. The droplet emerges on the solid wall as a spherical cap with the contact angle θ . Since the droplet nucleation occurs at the liquid–solid interface with 3D characteristics, we adopt the Cartesian coordinate with the initial density profile

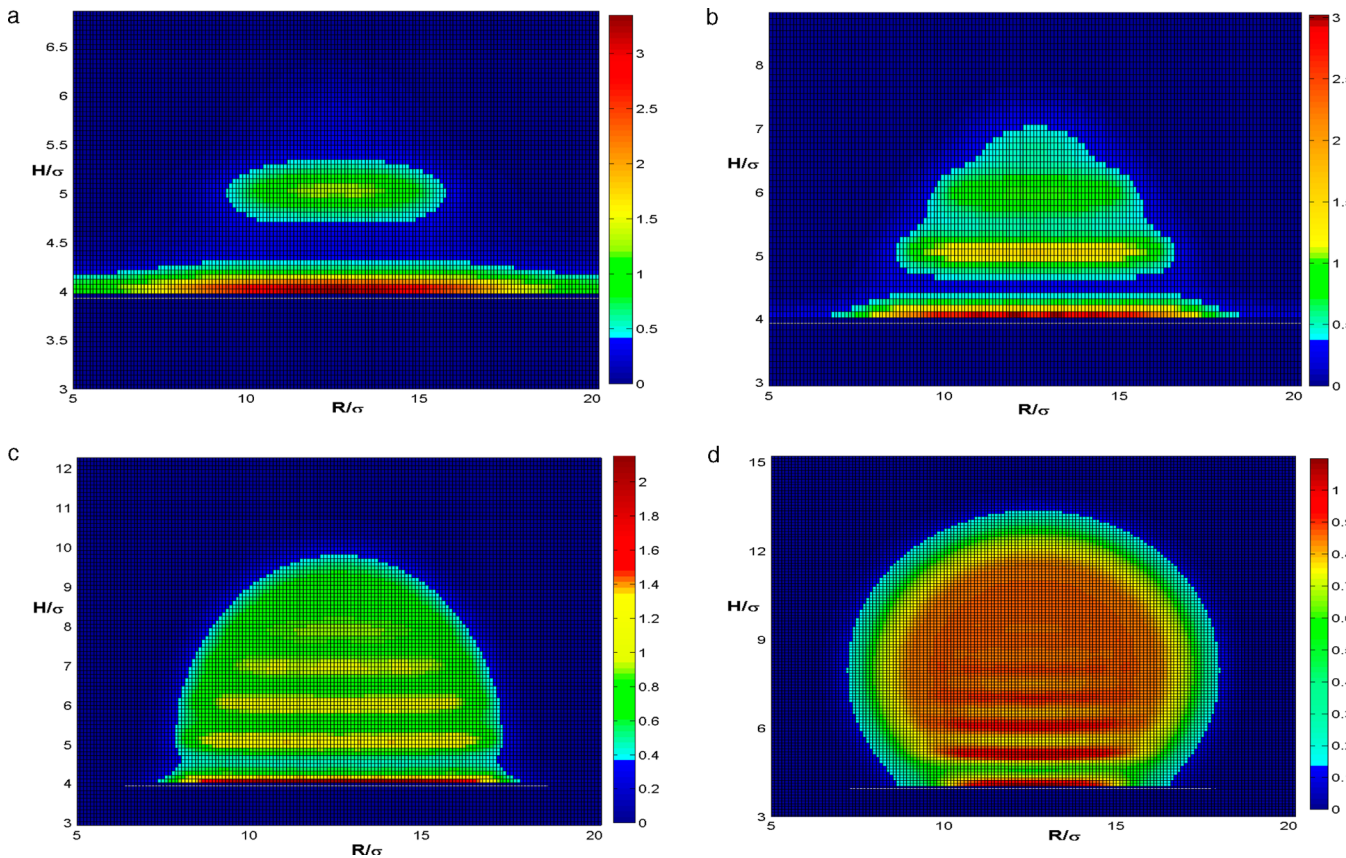


Figure 5. Overlook sketch of the critical nucleus and the density fluctuation of droplet formation on different walls. (a) $\theta = 70^\circ$ and $R_c = 3.58\sigma$, (b) $\theta = 90^\circ$ and $R_c = 3.92\sigma$, (c) $\theta = 120^\circ$ and $R_c = 4.44\sigma$, and (d) $\theta = 170^\circ$ and $R_c = 4.94\sigma$. The profiles are cut at $x = 12.8\sigma$.

$$\rho(x, y, z) = \begin{cases} 0 & z \leq z_0 \\ \rho_1 & r \leq R_0 \\ \rho_{sv} & r > R_0 \end{cases} \quad (17)$$

where z_0 is the position of the solid wall for the boundary effects and R_0 is the initial radius of the nucleus with r the distance to the center of the spherical cap. ρ_1 is the equilibrium liquid density, and ρ_{sv} denotes the density of the supersaturated vapor. In the numerical calculations, the system is discretized into $256 \times 256 \times 256$ grids and the grid spacing is 0.1σ in each direction. Accordingly, eq 4 can be solved using the Picard iteration. The iteration procedure is repeated until the average fractional difference over any 3D grid point between the old and the new 3D density function is less than 10^{-4} . According to a determined density profile, the interface of the droplet on the solid wall is the position of the interfacial density, i.e., $(\rho_1 + \rho_{vs})/2$. The distance between the interface at $x = 12.8\sigma$ and $y = 12.8\sigma$ and the center of the solid substrate is the height H of the droplet with contact angle θ . The radius of the droplet is defined as $R = H/(1 - \cos \theta)$ for $\theta \leq 90^\circ$ and $R = H/(1 + \cos(\pi - \theta))$ for $\theta > 90^\circ$.

Once the density profile has been obtained, the constrained free energy for heterogeneous nucleation can be calculated by

$$\begin{aligned} \Delta\Omega &= \Omega + pV \\ &= k_B T \int d\mathbf{r} \rho(\mathbf{r}) [\ln(\rho(\mathbf{r})\Lambda^3) - 1] + F_{hs}[\rho(\mathbf{r})] \\ &\quad + F_{att}[\rho(\mathbf{r})] + \int d\mathbf{r} [\rho(\mathbf{r})(V_{ext}(\mathbf{r}) - \mu)] + pV \end{aligned} \quad (18)$$

where V is the volume of the system.

As the constrained free energy of the droplet formation reaches a maximum, the size of the droplet is defined as the critical radius R_c and the maximum energy is the nucleation barrier.

We note that, for vapor–liquid–solid three–phase contact systems, previous DFT approaches^{22,33,34} calculate the liquid–solid, vapor–solid, and vapor–liquid interfacial tensions independently. More importantly, the three-phase contact line tension is either neglected³³ or described with other theoretical approaches.^{35–37} In contrast, the free energy in our 3D approach is a complete form, where the liquid–solid, vapor–solid, and vapor–liquid interfacial tensions, as well as the line tension are entirely included.

3. RESULTS AND DISCUSSION

We would like to get insight into the heterogeneous nucleation by analyzing four fluid–wall systems with different solvophilic characteristics. All the results are calculated at $T^* = k_B T/\epsilon = 0.70$ and the supersaturation ratio S is 2.0 for nucleation. The energy parameters for fluid–wall interactions are 0.80ϵ , 0.65ϵ , 0.42ϵ , and 0.14ϵ , respectively. The independent liquid–solid, vapor–solid, and vapor–liquid interfacial tensions of equilibrium LJ fluid in contact with different walls can be easily calculated by the DFT with its one-dimensional (1D) form. Accordingly, the contact angle θ can be approximately estimated by Young's equation. The corresponding values are 70° , 90° , 120° , and 170° , respectively. In the 3D calculation, the position of solid walls is all set at $z_0 = 3\sigma$ in consideration of the boundary effect.

We first examine the reliability of the theoretical approach. A convenient method is to compare the calculation results by

3D-DFT with those by 1D-DFT for symmetrical system, since the latter has been well validated. The density ρ^* in the following is dimensionless and defined as $\rho^* = \rho\sigma^3$.

Figure 1 presents the density distributions of the bulk liquid on the solvophilic ($\epsilon_{fw} = 0.80\epsilon$) and supersolvophobic ($\epsilon_{fw} = 0.14\epsilon$) walls, respectively. The data for 3D-DFT are derived from the center of solid walls ($x = 12.8\sigma$ and $y = 12.8\sigma$). Due to the symmetry, the density profile in 3D space can be simplified to 1D pattern. One can see that the 3D results agree well with the 1D ones. Another examination is carried out for homogeneous nucleation. Figure 2 represents the properties of the homogeneous nucleation of LJ fluid at $T^* = 0.70$ and $S = 2$. In Figure 2a, the two-dimensional cut of the density distribution of critical nucleus is given through the 3D-DFT calculation. The local densities in the droplet are almost uniform. Meanwhile, the free energy landscape is shown in Figure 2b for comparison with the results of 1D. From this figure, the same critical radius $R_c = 5.00\sigma$ is obtained from 1D and 3D approaches, and the free energy curves coincide well with each other before the critical nucleation, and a slight difference after the critical radius. Although the critical free energy for 3D is slightly higher than that for 1D, the deviation is within acceptable range. Figures 1 and 2 suggest that the present 3D model is capable of describing the inhomogeneous properties of LJ fluid.

In order to understand the mechanism of heterogeneous nucleation, the growth of a new droplet condensed from supersaturated vapor is investigated. As an example, the density distributions of nuclei of different sizes on the supersolvophobic surface ($\theta = 170^\circ$) are presented in Figure 3a–c to represent different stages of nucleation. The nucleus radii are 2.57σ , 3.56σ , and 4.94σ , respectively. Figure 3a shows the small cluster at the initial stage of nucleation. It can be seen that the density fluctuation in the nucleus is pronounced, and the layered structure dominates the whole shape of the droplet. In particular, the layered structure displays the depletion effect, which is induced by the surface force between the solvophobic wall and liquid droplet. Figure 3b shows the larger cluster than that in Figure 3a before the critical nucleation, and a platform emerges in the droplet. Compared with Figure 3a, the depletion effect decreases, and the densities in the first and second layers increase. The results may be determined by the competition between the surface force and the curvature. The critical nucleus is shown in Figure 3c. As the curvature of droplet decreases, and the first peak of droplet becomes higher than the second one. From the three nuclei, one can see that the first peak appears at σ from the solid wall ($z = 4\sigma$), and successive peaks arise at intervals of σ , and the peak almost disappears after the third one. The density profiles of the droplet are simply determined by the effective potential field.

Further illustration of the whole morphology of critical droplet is given in Figure 4. According to the above definition, the interfacial density is 0.42 under the nucleation condition, thereby the figure shows the sites in the droplet with $\rho^* \geq 0.42$. One can see that the droplet on the wall is a spherical cap shape.

The structures of nucleation droplet on different walls are further analyzed. Figure 5 presents the overlook sketch of the critical nucleus and the density fluctuations of different droplets at $x = 12.8\sigma$. From Figure 5a–d, the critical nucleus radii are 3.58σ , 3.92σ , 4.44σ , and 4.94σ , corresponding to 70° , 90° , 120° , and 170° , respectively. With the strong fluid–wall interaction $\epsilon_{fw} = 0.80\epsilon$, a spread of the first layer is significant in Figure 5a. The highest density in the droplet approaches to 3.2. It can be also observed that, with the decreasing strength of the interaction potential, more drying shape is formed, and the droplet is

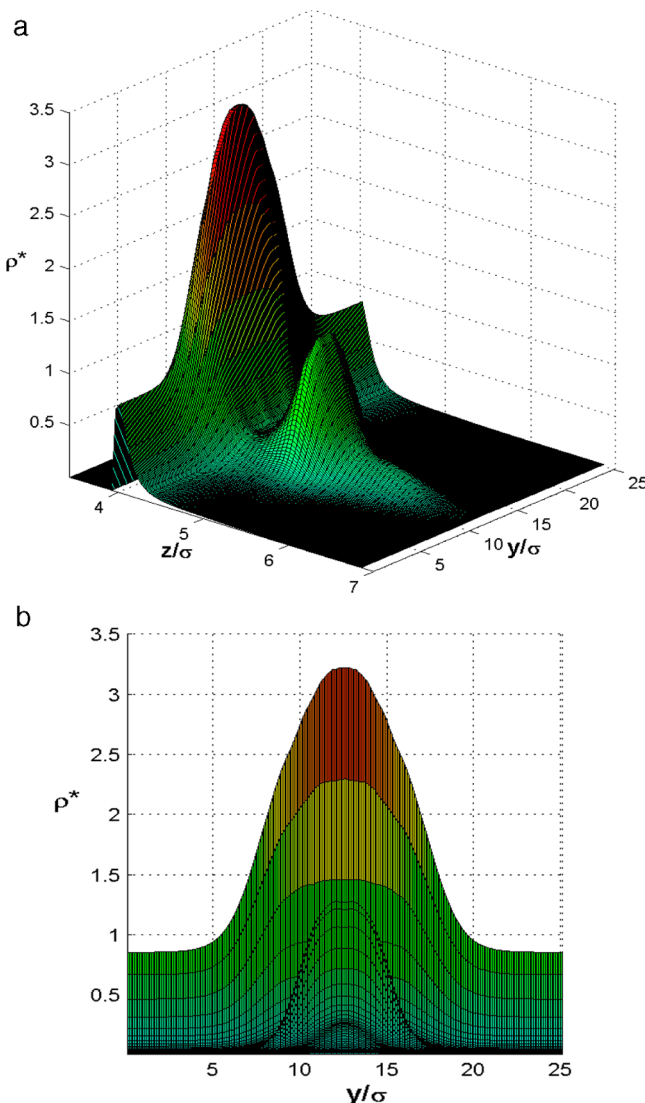


Figure 6. Full view of two-dimensional density profile of the critical droplet and the surrounding supersaturated vapor and on the solvophilic wall with $\theta = 70^\circ$. (a) Lateral view and (b) front elevation view. The profiles are cut at $x = 12.8\sigma$.

gradually close to the state of homogeneous nucleation. Under the supersolvophobic condition $\epsilon_{fw} = 0.14\epsilon$, the highest density decreases to about 1.1.

To clearly observe the density distribution of the droplet on the solvophilic wall, the lateral view and the front elevation view of Figure 5a are shown in Figure 6. As shown in Figure 6a, two peaks emerge for $\epsilon_{fw} = 0.80\epsilon$, and the first peak in the droplet is higher than the second one. In Figure 6b, outside the droplet, it is the adsorption of the supersaturated vapor near the solid wall, which is the same as that before phase transition.

Figure 7 shows the free energy landscape of heterogeneous nucleation on above solid walls, and the free energy of the homogeneous nucleation is also revealed. $\Delta\Omega$ for each curve has a local maxima at $R = R_c$, which correlates to a state of unstable equilibrium. When a cluster has a radius R less than R_c , any increase of R corresponds to an increase in $\Delta\Omega$, indicating that the cluster would shrink. On the other hand, when a cluster has a radius larger than R_c , any increase in R corresponds to a decrease of $\Delta\Omega$ indicating that the droplet would grow up. Figure 7 shows that as contact angle increases, the critical nucleus radius

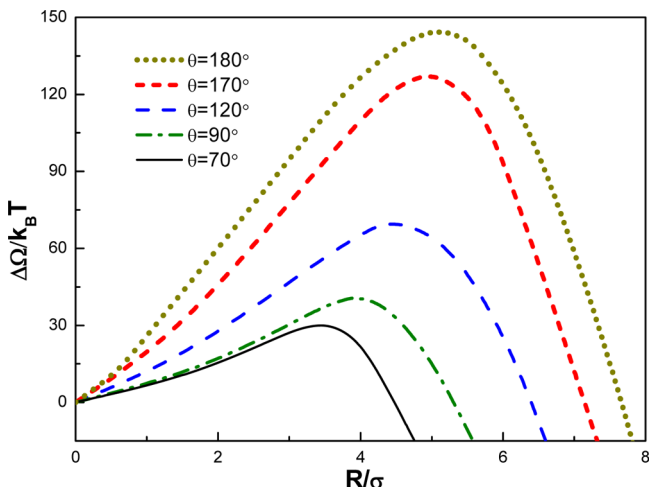


Figure 7. Constrained free energy curves of the growing droplets on different walls.

increases and the nucleation barrier becomes larger, and thus the droplet nucleation becomes more difficult. The reliability of the results can be evaluated by the homogeneous nucleation, which can be considered as a special heterogeneous nucleation in completely solvophobic state. Since the critical nucleus radius and the free energy barrier for homogeneous nucleation have been tested to be reliable by the DFT²⁵ and their varying trends are consistent with nucleation law, we can conclude that the results for heterogeneous nucleation are also reliable.

4. CONCLUSIONS

We provide a 3D-DFT approach to investigate heterogeneous nucleation of LJ fluid on different solid walls. The corresponding critical nucleus radii and the free energy barriers for condensation of supersaturated vapor into a droplet have been obtained. The reliability of the theoretical approach has been validated in symmetrical systems, including homogeneous nucleation and density profiles of liquid in contact with walls. In particular, the density distributions inside the nucleus have been presented to analyze the growing process of the nucleated droplet. According to its 3D characteristic, the present theoretical approach can be easily applied to study droplet or bubble nucleation on rough surfaces. As a result, this work contributes to the development of heterogeneous nucleation theory.

■ AUTHOR INFORMATION

Corresponding Author

*E-mail: mijg@mail.buct.edu.cn.

Notes

The authors declare no competing financial interest.

■ ACKNOWLEDGMENTS

This work is supported by National Natural Science Foundation of China (No. 21076006) and by Chemcloudcomputing of Beijing University of Chemical Technology.

■ REFERENCES

- (1) Leach, R. N.; Stevens, F.; Langford, S. C.; Dickinson, J. T. *Langmuir* **2006**, *22*, 8864–8872.
- (2) Family, F.; Meakin, P. *Phys. Rev. Lett.* **1988**, *61*, 428–431.
- (3) Narhe, R. D.; Khandkar, M. D.; Adhi, K. P.; Limaye, A. V.; Sainkar, S. R.; Ogale, S. B. *Phys. Rev. Lett.* **2001**, *86*, 1570–1573.
- (4) Winter, D.; Virnau, P.; Binder, K. *Phys. Rev. Lett.* **2009**, *103*, 225703.
- (5) Volmer, M. Z. *Elektrochem.* **1929**, *35*, 555.
- (6) Gretz, R. D. *J. Chem. Phys.* **1966**, *45*, 3160–3161.
- (7) Talanquer, V.; Oxtoby, D. W. *J. Chem. Phys.* **1996**, *104*, 1483–1492.
- (8) Lauri, A.; Zapadinsky, E.; Vehkamaki, H.; Kulmala, M. *J. Chem. Phys.* **2006**, *125*, 164712.
- (9) Erdemir, D.; Lee, A. Y.; Myerson, A. S. *Acc. Chem. Res.* **2009**, *42*, 621–629.
- (10) Kimura, T.; Maruyama, S. *Microscale Thermophys. Eng.* **2002**, *6*, 3–13.
- (11) Maruyama, S.; Kimura, T.; Lu, M.-C. *Therm. Sci. Eng.* **2002**, *10*, 23–29.
- (12) Rozas, R.; Kraska, T. *J. Phys. Chem. C* **2007**, *111*, 15784–15791.
- (13) Winter, D.; Virnau, P.; Binder, K. *J. Phys.: Condens. Matter* **2009**, *21*, 464118.
- (14) Davis, H. T. *Statistical Mechanics of Phases, Interfaces and Thin Films*; Wiley-VCH: Weinheim, Germany, 1996.
- (15) Rowlinson, J. S.; Widom, B. *Molecular Theory of Capillarity*; Oxford University Press: Oxford, U.K., 1989.
- (16) Bykov, T. V.; Zeng, X. C. *J. Chem. Phys.* **2002**, *117*, 1851–1868.
- (17) Bykov, T. V.; Zeng, X. C. *J. Chem. Phys.* **2006**, *125*, 144515.
- (18) Ruckenstein, E.; Nowakowski, B. *J. Colloid Interface Sci.* **1990**, *137*, 583–592.
- (19) Ruckenstein, E.; Nowakowski, B. *Langmuir* **1991**, *7*, 1537–1541.
- (20) Nowakowski, B.; Ruckenstein, E. *J. Phys. Chem.* **1992**, *96*, 2313–2316.
- (21) Berim, G. O.; Ruckenstein, E. *J. Colloid Interface Sci.* **2011**, *355*, 259–264.
- (22) Zeng, M.; Mi, J.; Zhong, C. *Phys. Chem. Chem. Phys.* **2011**, *13*, 3932–3941.
- (23) Yu, Y.-X.; Wu, J. *J. Chem. Phys.* **2002**, *117*, 10156–10164.
- (24) Kim, S.-C.; Lee, S. H. *J. Phys.: Condens. Matter* **2004**, *16*, 6365–6374.
- (25) Zhou, D.; Zeng, M.; Mi, J.; Zhong, C. *J. Phys. Chem. B* **2011**, *115*, 57–63.
- (26) Kuni, F. M.; Shchekin, A. K.; Rusanov, A. I.; Widom, B. *Adv. Colloid Interface Sci.* **1996**, *65*, 71–124.
- (27) Knepley, M. G.; Karpeev, D. A.; Davidovits, S.; Eisenberg, R. S.; Gillespie, D. *J. Chem. Phys.* **2010**, *132*, 124101.
- (28) Trudeau, T. G.; Jena, K. C.; Hore, D. K. *J. Phys. Chem. C* **2009**, *113*, 20002–20008.
- (29) Barker, J. A.; Henderson, D. *J. Chem. Phys.* **1967**, *47*, 2856–2861.
- (30) Barker, J. A.; Henderson, D. *J. Chem. Phys.* **1967**, *47*, 4714–4721.
- (31) Tang, Y.; Wu, J. *Phys. Rev. E* **2004**, *70*, 011201.
- (32) Tang, Y.; Tong, Z.; Lu, B. C.-Y. *Fluid Phase Equilib.* **1997**, *134*, 21–42.
- (33) Van Swol, F.; Henderson, J. R. *Phys. Rev. A* **1991**, *43*, 2932–2942.
- (34) Bauer, C.; Dietrich, S. *Eur. Phys. J. B* **1999**, *10*, 767–779.
- (35) Widom, B. *J. Phys. Chem.* **1995**, *99*, 2803–2806.
- (36) Bresme, F.; Quirke, N. *Phys. Rev. Lett.* **1998**, *80*, 3791–3794.
- (37) Koga, K.; Widom, B. *J. Chem. Phys.* **2007**, *127*, 064704.